ACS Partner Journal

CHEMICAL & BIOMEDICAL IMAGING

Open Access

pubs.acs.org/ChemBioImaging

Article

Screening Anti-Parkinson's Disease Drugs in Living Mouse Brains via a Peroxynitrite-Activated Fluorescent Probe

Jiao Wu,[†] Xiaoyu Wang,[†] Jingwen Zou, Renli Qiu, Zhiqiang Mao,* and Zhihong Liu*

Cite This: *Chem. Biomed. Imaging* 2025, 3, 301−309

Read Online

ACCESS | Metrics & More | Article Recommendations | Supporting Information

ABSTRACT: Screening anti-Parkinson's disease (PD) drugs at *in vivo* brain level is imperative for managing PD yet currently remains unaccomplished. Peroxynitrite ($ONOO^-$) has been implicated in PD progression. Thus, developing *in vivo* $ONOO^-$-based imaging tools for anti-PD drug screening holds promise for early prognosis and treatment of PD. Consequently, a near-infrared (NIR) fluorescence probe, **BOB-Cl-PN**, with high specificity, good sensitivity (LOD = 24 nM), and rapid response (<60 s), was devised to investigate $ONOO^-$ and PD relationships. Utilizing NIR fluorescence imaging, **BOB-Cl-PN** effectively monitored $ONOO^-$ fluctuations in 1-methyl-4-phenyl-1,2,3,6-tetrahydropyridine (MPTP)-induced PD cell models, establishing a cellular high throughput screening (cHTS) system for anti-PD drugs. In live animal imaging, **BOB-Cl-PN**'s ability to penetrate the blood−brain barrier enabled $ONOO^-$ flux imaging of PD mouse brains. Moreover, **BOB-Cl-PN** served as an imaging contrast for *in vivo* screening of potential traditional Chinese medicines for PD therapy, identifying fisetin as having the best therapeutic index among 10 Chinese medicines. This study constructs a sensitive, efficient imaging contrast for monitoring $ONOO^-$ dynamics in PD brains and provides a valuable platform for cellular and *in vivo* screening of anti-PD drugs.

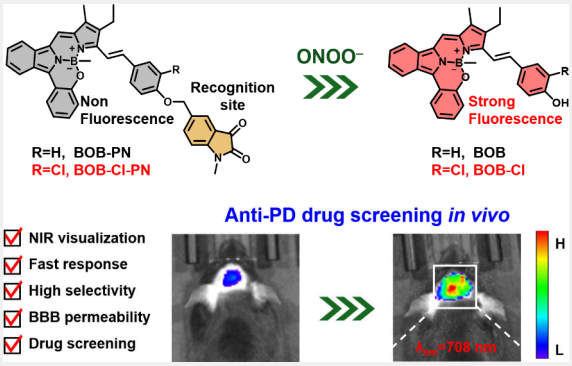

KEYWORDS: *Parkinson's disease, brain disease, fluorescent probe, peroxynitrite, Chinese medicine*

INTRODUCTION

Parkinson's disease (PD) is the second most common neurodegenerative disease in middle-aged and older adults, following Alzheimer's disease.[1] The pathological features of PD involve the degeneration and death of dopaminergic neurons in the midbrain substantia nigra, resulting in a significant decrease in dopamine activity and content.[2,3] Currently, PD cannot be completely cured and can only be managed with medications to alleviate the progression of the disease, placing a heavy burden on families worldwide. Consequently, there is an urgent need to explore more potential therapeutic drugs to ameliorate or even cure the disease.[4,5] Comparatively to the studies focusing on drug action mechanism and the Trial and Error methods employed in screening PD drugs, fluorescent probes have emerged as a highly promising approach in recent years.[6−9] This is primarily attributed to their noteworthy advantages of high sensitivity, exceptional specificity, and the ability to noninvasively monitor drug effects in real-time.[10−16]

Thus, the use of fluorescent probes for PD drug screening and discovery furnished the following three primary advantages: (1) By leveraging the power of fluorescent probe-based imaging technology, it becomes feasible to establish a readily accessible platform for high-throughput drug screening. Such a platform enables the rapid evaluation and screening of a vast number of potential drug candidates.[17−20] Consequently, this expedites the overall drug research and development process while simultaneously reducing the costs associated with drug discovery. (2) Fluorescent probes have the ability to bind to PD-associated biomolecules such as proteins, metal ions, and reactive species.[21−25] By utilizing real-time fluorescence imaging, they can assess drug affinity, selectivity, and potential side effects by monitoring the interactions between drugs and these targets. (3) Fluorescent probe-based imaging enables the observation of drug distribution, metabolism, and transport processes within cells or living animals.[26−29] This technique offers researchers a valuable means to visualize the mechanisms of drug action, optimize drug design, and enhance its efficacy.

Peroxynitrite ($ONOO^-$) is recognized as a potent oxidant and neurotoxic factor, considered pivotal in the development of neurodegenerative diseases.[30−32] Studies indicate a notable increase in $ONOO^-$ concentration in the brains of PD patients, underscoring the importance of accurately detecting $ONOO^-$ levels to comprehend PD progression. For instance,

Received: September 27, 2024
Revised: November 22, 2024
Accepted: November 23, 2024
Published: December 20, 2024

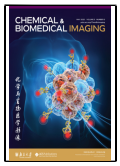

https://doi.org/10.1021/cbmi.4c00076
Chem. Biomed. Imaging 2025, 3, 301−309

Scheme 1. (A) Design Principles of Probe. (B) Mechanism of BOB-Cl-PN Response to $ONOO^-$ in Parkinson's Disease Mice

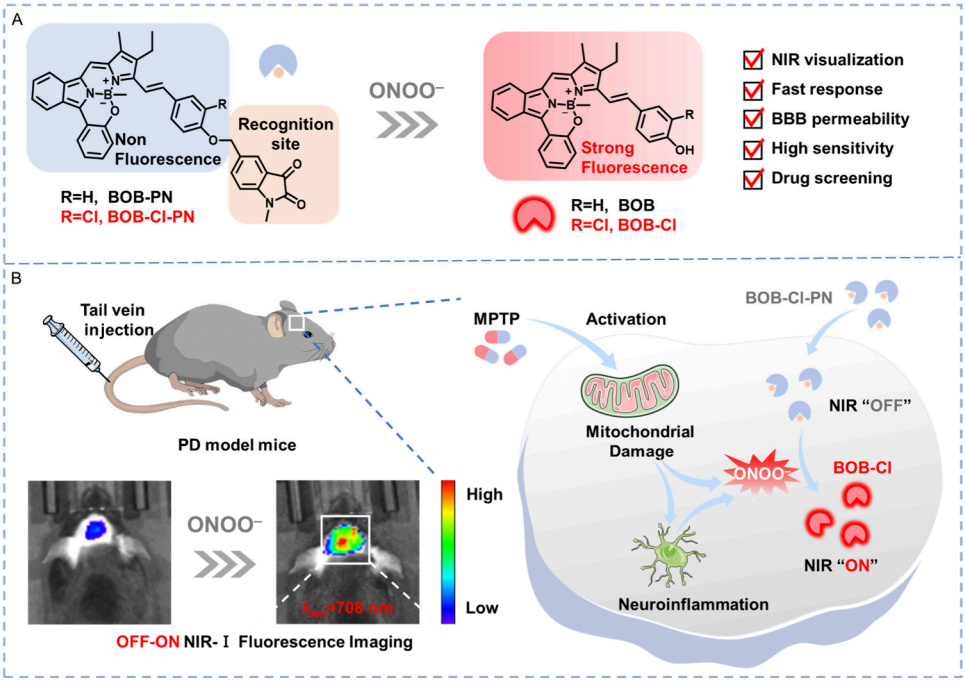

in 2020, Liu's team devised a series of NIR fluorescent probes (**NIR-PN**s) with ultrafast $ONOO^-$ response, enabling visualization of $ONOO^-$ fluctuations in PC12 cells, *Drosophila*, *C. elegans*, and PD mouse brains.[33] Similarly, in the same year, Li's group introduced a two-photon fluorescent probe (**ER-PN**) for imaging endoplasmic reticulum $ONOO^-$ in living cells and a PD model of the nematode *Hidradenitis elegans*.[34] In 2022, Zhang and colleagues developed a ratiometric NIR fluorescent probe successfully monitoring $ONOO^-$ fluctuations in a zebrafish PD model.[35] Until now, only a limited number of probes have been able to be utilized for *in vivo* imaging of $ONOO^-$ in PD mice.[36−39] Furthermore, there is little mention of their application in estimating anti-PD drug screening through *in vivo* fluorescence, potentially due to the inadequate permeability of the blood−brain barrier (BBB) and subpar real-time imaging capabilities of current probes.[40−42] Consequently, it is crucial to develop fluorescent probes that possess both enough BBB-permeability and high sensitivity, allowing for the real-time monitoring of dynamic changes in cerebral $ONOO^-$.

In this study, we report a near-infrared (NIR) $ONOO^-$-activated fluorescent probe **BOB-Cl-PN**, enables the real-time imaging of $ONOO^-$ in PD mouse brains and facilitates *in vivo* screening of anti-PD drugs. **BOB-Cl-PN** demonstrates outstanding selectivity, high sensitivity, and rapid response to $ONOO^-$ in solution tests with an emission peak at 708 nm. Cellular imaging results support that **BOB-Cl-PN** can sensitively detect intracellular $ONOO^-$ variations induced by incubating cells with $ONOO^-$ donors or lipopolysaccharide (LPS), as well as in a PD cell model. Additionally, a high-throughput screening (HTS) platform has been developed to assess the therapeutic efficacy of anti-PD drugs at the cellular level using cell culture plates. Further, through *in vivo* brain imaging, **BOB-Cl-PN** facilitates the screening of effectual anti-PD drugs from ten Chinese herbal medicines by utilizing real-time fluorescence associated with $ONOO^-$ in mice. Overall, this work introduces a valuable tool for early PD diagnosis and real-time screening of potential anti-PD drugs using NIR fluorescence imaging.

EXPERIMENTAL SECTION

Experimental Details

Details of the experiment are given in the Supporting Information.

Synthesis of BOB-Cl-PN

In a 50 mL round-bottomed flask, 173 mg (0.34 mmol) **BOB-Cl**, 104.2 mg compound **4** and 140 mg anhydrous K_2CO_3 were added and dissolved by 20 mL DMF. It then reacts overnight at 80 °C. After the reaction, 40 mL pure water was added to quench the reaction, then the mixture was extracted with CH_2Cl_2 (60 mL × 3) and dried with anhydrous Na_2SO_4. The solvent is removed. The crude product was purified by silica gel column chromatography (eluent: dichloromethane/petroleum ether = 3:1, *v*:*v*) to obtain a dark blue solid powder (50 mg, 22% yield). ^{1}H NMR (400 MHz, DMSO-d_6) δ 8.41 (*d*, *J* = 8.2 Hz, 1H), 8.29 (*d*, *J* = 8.0 Hz, 1H), 8.22 (*d*, *J* = 8.1 Hz, 1H), 7.97 (*d*, *J* = 10.8 Hz, 3H), 7.87 (*d*, *J* = 16.8 Hz, 1H), 7.81 (*dd*, *J* = 8.2, 1.9 Hz, 1H), 7.75 (*d*, *J* = 2.2 Hz, 1H), 7.68 (*d*, *J* = 1.8 Hz, 1H), 7.64 (*dd*, *J* = 8.2, 6.9 Hz, 2H), 7.51 (*q*, *J* = 8.9, 8.4 Hz, 2H), 7.42 (*d*, *J* = 8.6 Hz, 1H), 7.23−7.18 (m, 2H), 7.11 (*d*, *J* = 8.6 Hz, 2H), 5.27 (*s*, 2H), 3.16 (*s*, 3H), 2.29 (*s*, 3H), 0.85 (*s*, 3H), −0.14 (*s*, 3H).

RESULTS AND DISCUSSION

Probe Design

The N_2O-type benzopyrromethene boron complex (BOBPY) was selected as the fluorophore scaffold for its locked planar structure and axial steric protection, which contribute to its exceptional stability, high absorbance, high fluorescence quantum yield, narrow emission band, and near-infrared emission.[43] Consequently, BOBPY fluorophores exhibit significant promise in the development of fluorescence probes.[44−46] Through the Knoevenagel condensation reaction, the methyl group of BOBPY was condensed with the aldehyde group of 4-hydroxybenzaldehyde to yield the new fluorescent compound, **BOB**. Recognizing that halogen substitution can notably influence the probe's response properties, a related

https://doi.org/10.1021/cbmi.4c00076
Chem. Biomed. Imaging 2025, 3, 301−309

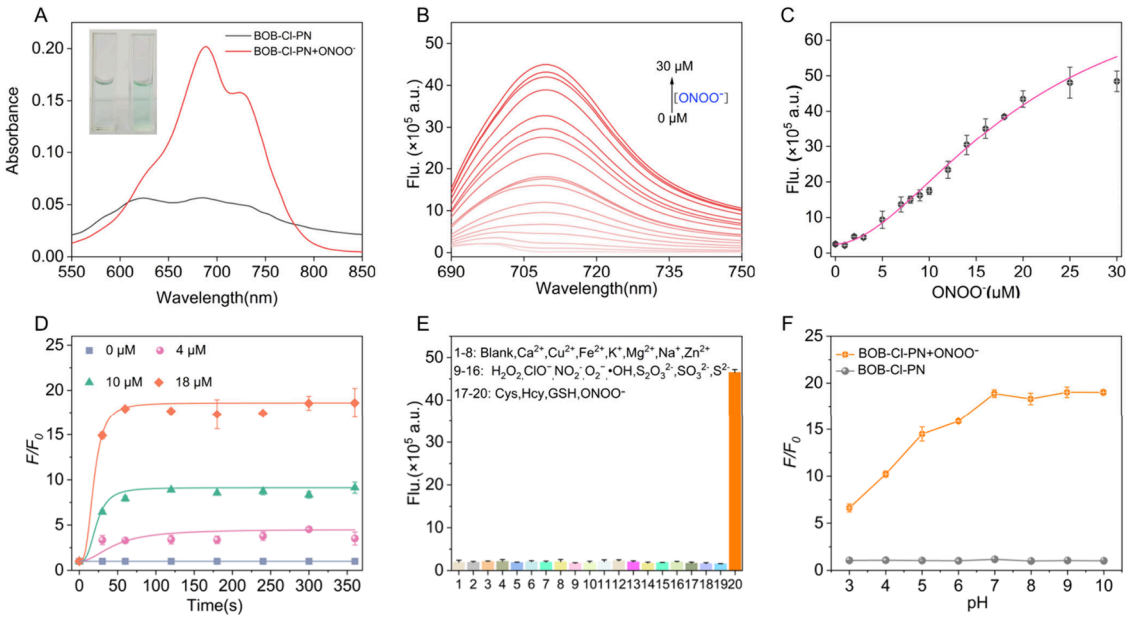

Figure 1. (A) Absorption spectra of **BOB-Cl-PN** before and after reacting with $ONOO^-$. Inset: color change of **BOB-Cl-PN** before (left) and after (right) reacting with $ONOO^-$. (B) Spectral response of 10 μM **BOB-Cl-PN** with 0−30 μM $ONOO^-$. (C) Relationship of fluorescence intensities and $ONOO^-$ concentrations. (D) Time course of fluorescence responses of **BOB-Cl-PN** with 0, 4, 10, 18 μM $ONOO^-$. (E) Fluorescence responses of 10 μM **BOB-Cl-PN** to various biological species including 20 μM **2**−**8**: Ca^{2+}, Cu^{2+}, Fe^{2+}, K^+, Mg^{2+}, Na^+, Zn^{2+}; 50 μM **9**−**16**: H_2O_2, ClO^-, NO_2^-, O_2^-, $^{\bullet}OH$, $S_2O_3^{2-}$, S^{2-}, SO_3^{2-}, 100 μM **17**−**19**: Cys, Hcy, GSH, and 20 μM $ONOO^-$. (F) Influences of pH on the fluorescence response of **BOB-Cl-PN** to $ONOO^-$. $\lambda_{ex}/\lambda_{em}$ = 688/708 nm.

fluorophore, **BOB-Cl**, was synthesized by introducing a chlorine (Cl) atom into the *ortho* position of **BOB**'s phenol group. The hydroxyl group of the fluorophore (**BOB**, **BOB-Cl**) was linked with the $ONOO^-$ recognition unit 5-(bromomethyl)-1-methylindoline-2,3-dione to produce the probes **BOB-Cl-PN** and **BOB-PN**. Consequently, the fluorescence of the fluorophores in these two probes (**BOB-Cl-PN**, **BOB-PN**) was quenched by the isatin moiety.[47−49] Upon the probe's reaction with $ONOO^-$, the removal of the isatin component results in the liberation of the fluorophores **BOB**/**BOB-Cl**, thus reinstating strong near-infrared emission (Scheme 1). The synthesis and characterizations (^{1}H NMR and HRMS) of these probes are detailed in the Supporting Information (Scheme S1 and Figure S10−23).

Fluorescence Response to $ONOO^-$

First, the absorption and fluorescence responses of **BOB-Cl-PN** and **BOB-PN** to $ONOO^-$ were respectively measured in a PBS/DMF buffer solution (PBS, pH = 7.4, containing 50% DMF, *v*/*v*). The absorption peak of **BOB-PN** is at 688 nm. After the reaction with $ONOO^-$, the absorption peak position of **BOB-PN** is red-shifted to 730 nm (Figure S1A). The absorption peak of **BOB-Cl-PN** is located at 688 nm, and the absorbance undergoes a noticeable enhancement subsequent to the reaction with $ONOO^-$ (Figure 1A). At the same time, the fluorescence quantum yields of **BOB-Cl-PN** and **BOB-PN** before and after reaction with $ONOO^-$ were further evaluated (Table S1). Subsequently, the fluorescence spectra of **BOB-Cl-PN** and **BOB-PN** with varying concentrations of $ONOO^-$ were examined. Both probes exhibit a concentration-dependent increase in $ONOO^-$ fluorescence at 708 and 713 nm, respectively (Figures 1B and S1B). At an $ONOO^-$ concentration of 20 μM, the fluorescence intensity of **BOB-PN** increases approximately 4.5 times (F/F_0) (Figure S1B,C), revealing a strong linear relationship within the range of 7 to 15 μM $ONOO^-$ (Figure S2B). Furthermore, the limit of detection (LOD) was determined to be 1.39 μM using the $3\sigma/k$ method.

In contrast, the fluorescence intensity of **BOB-Cl-PN** at 708 nm is significantly enhanced upon interaction with $ONOO^-$ (Figure 1B), reaching a maximum F/F_0 value of approximately 19 times. Additionally, the fluorescence response within the range of 1.0 to 20 μM $ONOO^-$ demonstrates a strong linear relationship (Figure 1C). The calculated LOD value is 24 nM using the 3σ/k method (Figure S2A). It is evident that **BOB-Cl-PN** exhibits a much better response sensitivity to $ONOO^-$. Furthermore, the time-dependent relationship between the fluorescence profiles of **BOB-Cl-PN**/**BOB-PN** and $ONOO^-$ is also assessed. The fluorescence intensity of **BOB-Cl-PN** reached a plateau within 60 s upon the addition of 4.0−18 μM $ONOO^-$ (Figure 1D), whereas the reaction between **BOB-PN** and 3.0−20 μM $ONOO^-$ was completed within 120 s (Figure S1D). Thus, the reaction profiles demonstrate that **BOB-Cl-PN** reacts with $ONOO^-$ at a significantly faster rate compared to **BOB-PN**. The superior response performance of **BOB-Cl-PN**, characterized by a lower limit of detection (LOD) and rapid reaction rate, can be attributed to the enhanced reactivity and fluorescence resulting from the *ortho*-chlorine substitution.[50] The specificity of the probe for $ONOO^-$ detection is critical in complex biological environments. Therefore, we evaluated the selectivity of **BOB-Cl-PN** and **BOB-PN** for $ONOO^-$. As expected, no significant increase in fluorescence intensity was observed for the incubation of **BOB-PN** or **BOB-Cl-PN** with possible bio-interference substances (Figures 1E and S1E). Moreover, **BOB-Cl-PN** showed higher stability and specificity (19-fold vs 4.5-fold). It is worth noting that the co-incubation of 100 μM other ROS (ClO^-, H_2O_2, NO_2^-, $^{\bullet}OH$) also did not affect the response performance of the probes to $ONOO^-$, indicating that they have good anti-interference (Figure S3A,B). Finally, we further

https://doi.org/10.1021/cbmi.4c00076
Chem. Biomed. Imaging 2025, 3, 301−309

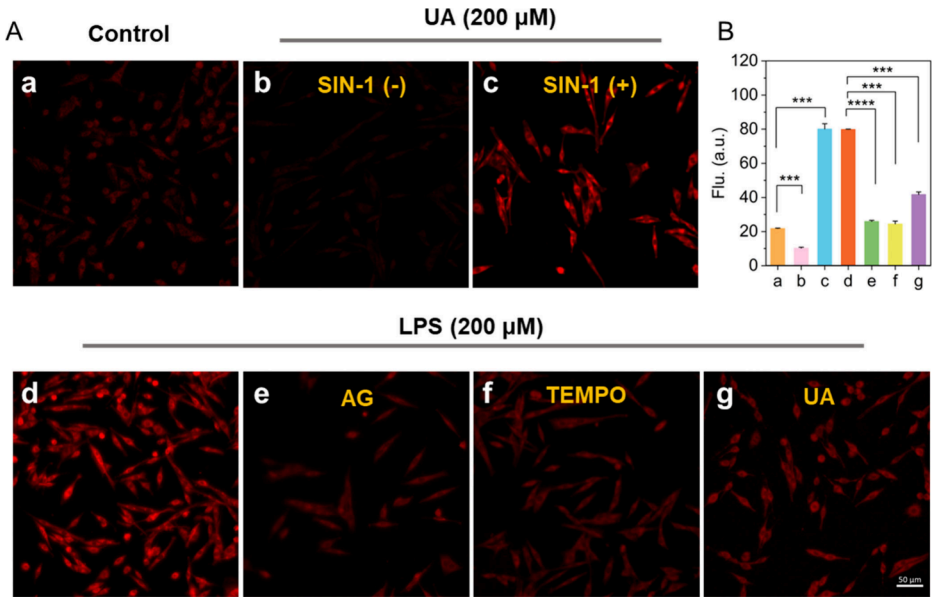

Figure 2. (A) (a) PC12 cells were incubated with **BOB-Cl-PN** (5 μM) for 0.5 h and then imaged. (b) PC12 cells were pretreated with UA (200 μM) for 0.5 h, then incubated with **BOB-Cl-PN** (5 μM) for 0.5h for imaging. (c) PC12 cells were pretreated with UA (200 μM) for 0.5 h, then incubated with **BOB-Cl-PN** (5 μM) and SIN-1 (800 μM) for 0.5 h for imaging. (d) PC12 cells were pretreated with UA (200 μM) for 0.5 h and incubated with LPS (2 μg/mL) for 4 h, then incubated with **BOB-Cl-PN** (5 μM) for 0.5 h for imaging. (e, f, g) PC12 ells were pretreated with (e) AG (200 μM), (f) TEMPO (200 μM), or (g) UA (200 μM) during stimulation with LPS (2 μg/mL) for 4 h, subsequently incubated with **BOB-Cl-PN** (5 μM) for 0.5 h and then imaged. (B) Mean intensities in a−g. Scale bar = 50 μm. λ_{ex} = 633 nm, λ_{em} = 650−749 nm. $^{**}p < 0.01$, $^{***}p < 0.001$, $^{****}p < 0.0001$.

evaluated the pH stability of the two probes. The fluorescence intensities of both probes and $ONOO^-$ remained stable at pH values of 7−10 and were higher than that at pH = 3−6 (Figures 1F and S1F). It may be due to the decomposition of $ONOO^-$ to produce $NO^•$ and $O_2^{-•}$ under acidic conditions below physiological pH and comprise the fluorescence decreases.[51,52] Through the test results, it can be concluded that **BOB-Cl-PN** showcases much more superior response performance, more suitable for the detection of $ONOO^-$ in complex biological environments. Further, we assessed the stability of **BOB-Cl-PN** in mouse plasma. After 11 h of incubation, **BOB-Cl-PN** still exhibited strong stability in plasma (Figure S4). Afterward, we summarize several $ONOO^-$-activated probes used for detecting PD, comparing their optical properties and biological applications (Figure S5 and Table S2). Notably, **BOB-Cl-PN** offers significant advantages over other probes in terms of near-infrared emission, penetration depth, and ability to cross the blood−brain barrier.

NIRF Imaging of Cellular $ONOO^-$

Prior to the imaging of the cells, we determined the cytotoxicity of **BOB-Cl-PN** on PC12 cells using the MTT assay. As shown in Figure S6, **BOB-Cl-PN** exhibited low cytotoxicity to living PC12 cells at low concentrations. According to the MTT results, the probe concentration of 5 μM was selected for subsequent cell experiments. Next, we investigated the cellular imaging capabilities of **BOB-Cl-PN**. Initially, the PC12 cells showed a weak fluorescence signal after the incubation with **BOB-Cl-PN** (Figure 2a). To eliminate the effect of endogenous $ONOO^-$, PC12 cells were pretreated with uric acid (UA, an $ONOO^-$ scavenger) and incubated with **BOB-Cl-PN** for confocal cell imaging. Weak fluorescence intensity was observed in the cells (Figure 2b). This proves that the fluorescence intensity in Figure 2a is induced by cellular endogenous $ONOO^-$. Additionally, PC12 cells were pretreated with UA to deplete endogenous $ONOO^-$ and stimulated with 3-morpholino-sydnonimine (SIN-1, exogenous $ONOO^-$ donor) or lipopolysaccharide (LPS, endogenous $ONOO^-$ stimulator). Compared with Figure 2b, the fluorescence intensity was significantly improved (Figure 2c,d,B). In order to verify the specificity of **BOB-Cl-PN** to $ONOO^-$, several $ONOO^-$ inhibitors were applied including aminoguanidine (AG, a commonly used NO synthase inhibitor), 2,2,6,6-tetramethylpethyl-1-oxide (TEMPO, a superoxide radical scavenger), and UA (Figure 2e,f,g, respectively).[53,54] The results indicated that the inhibitor significantly diminished fluorescence in comparison to the control group (Figure 2B), and **BOB-Cl-PN** could sensitively monitor the intracellular $ONOO^-$ level.

The neurotoxin 1-methyl-4-phenyl-1,2,3,6-tetrahydropyridine (MPTP) is recognized for inducing degeneration and necrosis of dopaminergic neurons by depleting adenosine triphosphate (ATP) and generating reactive oxygen species (ROS), consequently leading to a substantial decrease in dopamine levels.[55] Building upon this premise, we exposed PC12 cells to MPTP for 2 h to establish a PD cell model. As depicted in Figure 3a−c, the intracellular fluorescence intensity gradually increased with the escalating concentration of MPTP (200 μM, 300 μM) in comparison to the control group (Figure 3a,B). This observation suggests the generation of $ONOO^-$ during the burst of reactive oxygen species (ROS) burst induced by MPTP. Significantly, the addition of UA notably decreased the fluorescence intensity in the PD cell models, indicating the effective reduction of $ONOO^-$ levels in the cells by UA (Figure 3d,B). Therefore, it is evident that **BOB-Cl-PN** can accurately monitor the fluctuation of $ONOO^-$ levels in the PD cell model.

https://doi.org/10.1021/cbmi.4c00076
Chem. Biomed. Imaging 2025, 3, 301−309

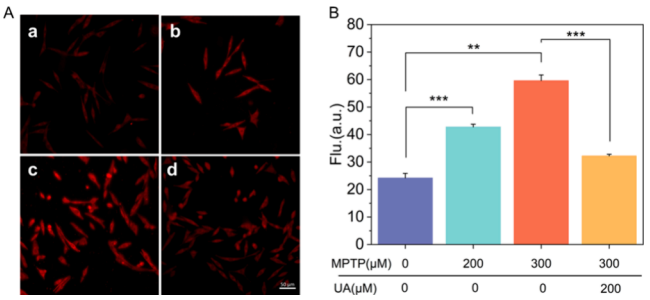

Figure 3. (A) NIRF imaging of $ONOO^-$ generated by the MPTP induced PD cells. 5 μM **BOB-Cl-PN** loaded cells were co-incubated with (a) 0 μM; (b) 200 μM; (c) 300 μM MPTP; (d) 300 μM MPTP + 200 μM UA. (B) Mean intensities in a–d. Scale bar = 50 μm. λ_{ex} = 633 nm, λ_{em} = 650–749 nm. $^{**}p < 0.01$, $^{***}p < 0.001$, $^{****}p < 0.0001$.

In Vivo Imaging of $ONOO^-$ Fluxes in PD Brains

Prior to in vivo imaging of $ONOO^-$ flux in the brains of PD mice, we measured the log *P* value of **BOB-Cl-PN** and measured a log *P* value of 1.8, suggesting that **BOB-Cl-PN** has the potential to cross the blood–brain barrier. To assess the potential of **BOB-Cl-PN** as an effective tool for real-time monitoring of $ONOO^-$ fluxes through fluorescence imaging in living mice, we employed C57BL/6 mice to establish PD models via intraperitoneal injection of MPTP for successive 6 days (Figure 4A). The MPTP-induced PD mice exhibited typical symptoms including the appearance of involuntary tremors in the body and a stiff erect tail, providing substantial evidence for the establishment of PD. Furthermore, Parkinson's disease is a neurodegenerative condition stemming from a reduction in dopamine levels within the substantia nigra striatum. Consequently, tyrosine hydroxylase (TH) plays a pivotal role in dopamine biosynthesis and is regarded as a biomarker for PD development.[56] Subsequently, immunofluorescence staining was conducted on the substantia nigra (SN) in the brain tissue of mice from the WT, PD, and treatment groups to evaluate the TH expression levels.

As illustrated in Figure 4F, TH expression in the substantia nigra of mice in the PD group was notably lower compared to that of WT mice. Following treatment with levodopa and amantadine, TH expression in the substantia nigra of PD mice

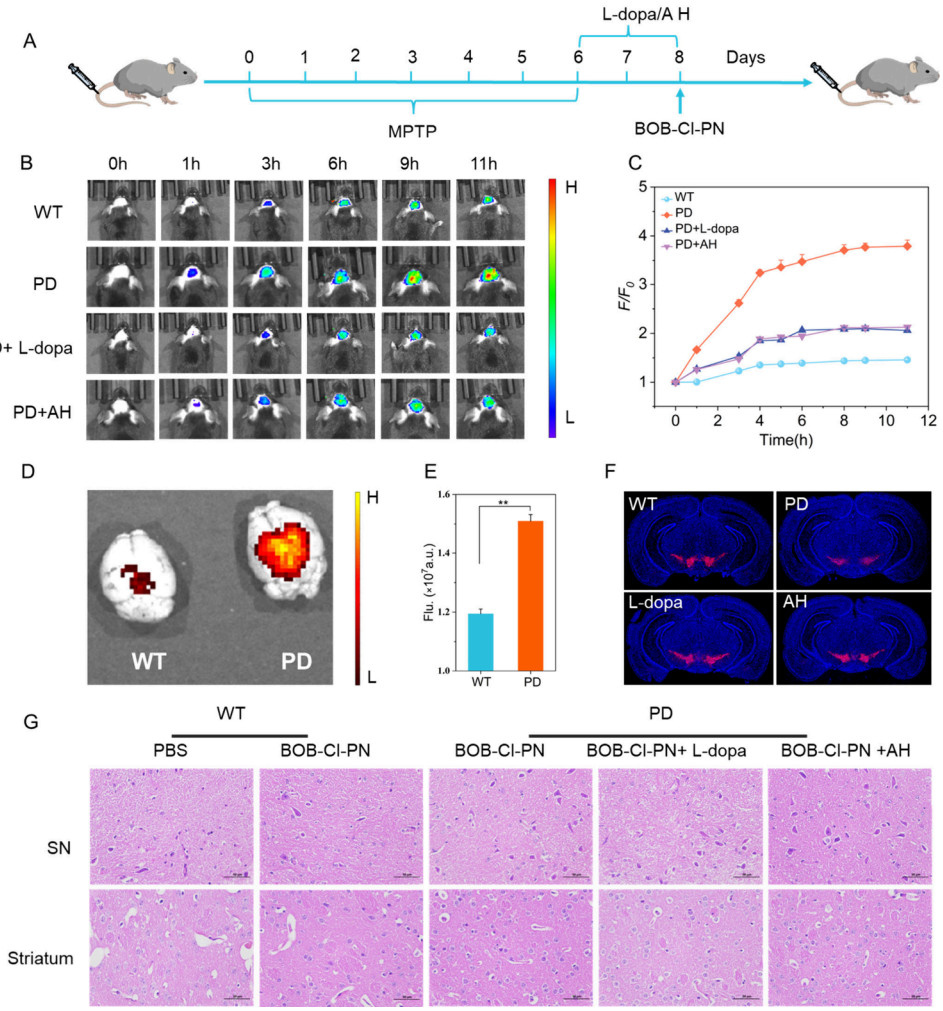

Figure 4. (A) Schematic diagram of the experimental timeline. (B) Fluorescence imaging of $ONOO^-$ in WT, PD, levodopa (L-dopa)-treated and amantadine hydrochloride (AH)-treated PD mice brains during 11 h via intravenous injection of **BOB-Cl-PN** (100 μL,10 μM). (C) Quantification of fluorescence signals in (A). (D) *Ex vivo* imaging of the brain from WT or PD mice postimaging. (E) *Ex vivo* fluorescence intensities of PD and WT mouse brains. (F) Immunofluorescence staining of substantia nigra in WT and PD mice. Scale bars: 1000 μm. (G) Hematoxylin and eosin staining of the substantia nigra and striatum. Scale bar = 50 μm. NIRF imaging: λ_{ex} = 680 nm, λ_{em} = 780 nm. N = 3, $^{**}p < 0.01$.

https://doi.org/10.1021/cbmi.4c00076
Chem. Biomed. Imaging 2025, 3, 301–309

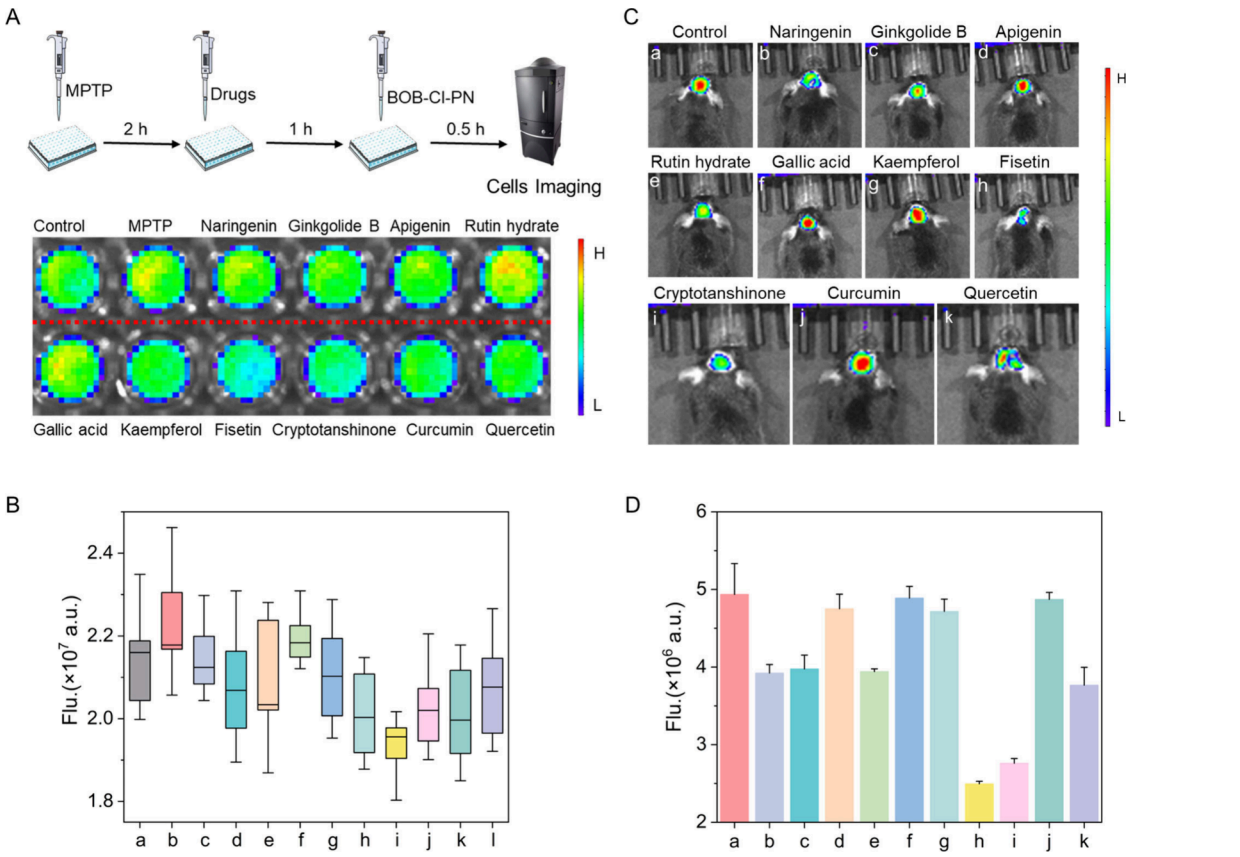

Figure 5. (A) Fluorescence imaging of PC12 cells treated with ten kinds of traditional Chinese medicines. (B) Box-plot expression of fluorescence intensity in A diagram (a−l: control, MPTP, naringenin, ginkgolide B, apigenin, rutin hydrate, gallic acid, kaempferol, fisetin, cryptotanshinone, curcumin, quercetin). (C) Fluorescence imaging of PD mice treated with Chinese medicine and **BOB-Cl-PN**. (D) Corresponding fluorescence intensities from (a−k). NIRF imaging: λ_{ex} = 680 nm, λ_{em} = 780 nm.

returned to normal levels. These findings strongly indicate the successful establishment of the PD mouse model.

For the *in vivo* imaging, following the tail vein injection of **BOB-Cl-PN** (10 μM), WT, PD, and drug-treated PD mice underwent real-time NIR fluorescence imaging for 11 h, respectively (Figures 4B and S7). As depicted in Figure 4B,C, time-dependent fluorescence imaging unveiled the differences in $ONOO^-$ concentration within the brains of mice across each group. The fluorescence intensity of PD mice notably increased within the 0−11 h (F_{max}/F_0 = 3.7). In contrast, only a slight fluorescence enhancement (F_{max}/F_0 = 1.45) was observed in the WT group. These results underscored the overexpression of $ONOO^-$ generation in PD brains. Simultaneously, real-time fluorescence imaging of the brains of PD mice administered with levodopa and amantadine hydrochloride, two prominent anti-PD drugs, revealed a significant reduction in the expression levels of $ONOO^-$ within the 0−11 h window compared to the PD group, approaching levels similar to those of WT mice (Figure 4B,C). These findings imply that **BOB-Cl-PN** can offer valuable insights for the treatment and drug development of PD by assessing $ONOO^-$ levels in the PD brain. Furthermore, *in vivo* NIR imaging was conducted on dissected brains from PD and WT mice. The fluorescence intensity in the PD brain exceeded that in the WT brain, illustrating the blood−brain barrier penetration capability of **BOB-Cl-PN** (Figure 4D,E). Finally, hematoxylin and eosin (H&E) staining was utilized to assess the biocompatibility of **BOB-Cl-PN**. Brain tissue slices from the substantia nigra (SN) and striatum of PD mice treated with **BOB-Cl-PN** displayed a resemblance to those from the PBS group, exhibiting no apparent damage (Figure 4G). And no notable alterations were observed in the hematoxylin and eosin (H&E) sections of heart, liver, spleen, lung, and kidney tissues from mice treated with **BOB-Cl-PN**, further affirming its exceptional biosafety (Figure S8). Thus, **BOB-Cl-PN** emerges as a promising tool, showcasing both excellent blood−brain barrier permeability and biocompatibility, for *in vivo* imaging of $ONOO^-$ in PD mouse model.

Screening of Traditional Chinese Medicine-Based Anti-PD Drugs in Cells and *In Vivo*

Having successfully tracked the dynamic changes of $ONOO^-$ content within the brains of PD mice, our investigation proceeded to evaluate the potential of **BOB-Cl-PN** as the vehicle for anti-PD drug screening. Ten traditional Chinese medicines, renowned for their redox regulatory and anti-inflammatory properties,[57,58] were individually combined with **BOB-Cl-PN** to conduct preliminary screening of potential PD treatment candidates. This screening involved observing the fluctuation of $ONOO^-$ levels using fluorescence imaging. We first constructed a high throughput screening (HTS) method for drug screening in the cell level. Briefly, MTTP-induced PD cells were cultured with 10 Chinese medicines and **BOB-Cl-PN** in a 72-well cell culture plate. And we can readily estimate the anti-PD therapeutic indexes of drugs through the *ex vivo* fluorescence imaging (Figure 5A). The HTS system with **BOB-Cl-PN** elicited that fisetin has the best therapeutic effects

https://doi.org/10.1021/cbmi.4c00076
Chem. Biomed. Imaging 2025, 3, 301−309

toward PD model cells (Figure 5B). For *in vivo* imaging-based drug screening, the control and PD mice were respectively injected with PBS and ten different traditional Chinese medicines via the tail vein over two consecutive days. One hour after the second-day injection of the therapeutic drug, all mice were administered 10 μM **BOB-Cl-PN** via the tail vein. Subsequently, the therapeutic effects of the different drugs were evaluated using *in vivo* brain fluorescence imaging. As illustrated in Figure 5C, 7 h postinjection of **BOB-Cl-PN**, the fluorescence intensity notably increased in PD mice injected with PBS alone. In comparison with the control group, apigenin, gallic acid, kaempferol, and curcumin induced minimal changes in fluorescence intensity, while naringin, ginkgolide B, rutin hydrate, cryptotanshinone, and quercetin resulted in a certain decrease in fluorescence intensity. However, the fluorescence intensity in PD mice injected with fisetin significantly decreased by approximately 1.9-fold compared to the control group (Figure 5D). This implies that fisetin may downregulate $ONOO^-$ expression in the brains of PD mice, potentially alleviating the MPTP-induced overproduction of $ONOO^-$ in the PD model. Subsequently, the substantia nigra region in the brain tissue of mice in the fisetin groups underwent immunofluorescence staining, and the therapeutic effect was assessed by observing the expression level of Tyrosine hydroxylase (TH). Surprisingly, after fisetin treatment, there was a significant increase in TH expression in the substantia nigra region of mice compared to control PD mice, indicating potential restoration of PD brains with fisetin administration (Figure S9). The probe-based *in vivo* imaging results align with the TH immunofluorescence findings, thus affirming the promising potential of the proposed anti-PD drug screening method using **BOB-Cl-PN**. Overall, **BOB-Cl-PN**, functioning as an imaging agent, not only sensitively monitors the dynamic changes of $ONOO^-$ in PD brains but also offers potential for in-cell or *in vivo* drug screening for PD treatment, marking a significant advancement in PD research.

CONCLUSION

In summary, we have developed the NIR fluorescence probe **BOB-Cl-PN** for tracking $ONOO^-$ fluctuations in PD brain models and establishing an $ONOO^-$-dependent anti-PD drug screening platform. **BOB-Cl-PN** exhibits excellent selectivity and sensitivity to $ONOO^-$, remarkable resistance to interference, and pH stability, along with a rapid response (<60 s) to $ONOO^-$, emitting a fluorescence signal at 708 nm. Moreover, **BOB-Cl-PN** accurately detects $ONOO^-$ flux in PC12 cells and MPTP-induced PD cell models through intracellular fluorescence imaging. Furthermore, thanks to its ability to cross the blood−brain barrier, **BOB-Cl-PN** has been successfully employed for real-time, *in vivo* imaging of $ONOO^-$ fluctuations in the brains of PD mice. Additionally, as a reliable imaging reagent, **BOB-Cl-PN** was utilized to screen traditional Chinese medicines for treating PD at both the cellular and mouse levels. The screening results reveal that fisetin may hold the most promise among the traditional Chinese medicines for alleviating PD and potentially offering therapeutic effects in the PD process. The exceptional $ONOO^-$-response performance and brain *in vivo* NIR fluorescence imaging capability of **BOB-Cl-PN** underscore its remarkable potential to aid in the early diagnosis and treatment of PD. Furthermore, it streamlines the process for *in vivo* and in-cellular anti-PD drug screening, offering a straightforward and effective approach.

ASSOCIATED CONTENT

Supporting Information

The Supporting Information is available free of charge at https://pubs.acs.org/doi/10.1021/cbmi.4c00076.

Experimental section, synthesis, optical properties of **BOB-Cl-PN** and **BOB-PN**, cytotoxicity, *in vivo* imaging of PD, H&E staining, immunofluorescence staining of substantia nigra, and NMR and MS spectra (PDF)

AUTHOR INFORMATION

Corresponding Authors

Zhiqiang Mao − *Hubei Province Key Laboratory of Biotechnology of Chinese Traditional Medicine, College of Health Science and Engineering, Hubei University, Wuhan 430062, China;* orcid.org/0000-0003-1766-8886; Email: maozq@hubu.edu.cn

Zhihong Liu − *Hubei Province Key Laboratory of Biotechnology of Chinese Traditional Medicine, College of Health Science and Engineering, Hubei University, Wuhan 430062, China;* orcid.org/0000-0003-1500-9342; Email: zhhliu@whu.edu.cn

Authors

Jiao Wu − *Hubei Province Key Laboratory of Biotechnology of Chinese Traditional Medicine, College of Health Science and Engineering, Hubei University, Wuhan 430062, China*

Xiaoyu Wang − *Hubei Province Key Laboratory of Biotechnology of Chinese Traditional Medicine, College of Health Science and Engineering, Hubei University, Wuhan 430062, China*

Jingwen Zou − *Hubei Province Key Laboratory of Biotechnology of Chinese Traditional Medicine, College of Health Science and Engineering, Hubei University, Wuhan 430062, China*

Renli Qiu − *Hubei Province Key Laboratory of Biotechnology of Chinese Traditional Medicine, College of Health Science and Engineering, Hubei University, Wuhan 430062, China*

Complete contact information is available at: https://pubs.acs.org/10.1021/cbmi.4c00076

Author Contributions

†Jiao Wu and Xiaoyu Wang contributed equally to this work.

Notes

The authors declare no competing financial interest.

ACKNOWLEDGMENTS

This work was financially supported by the National Natural Science Foundation of China (No. 22174034).

REFERENCES

(1) Hou, Y.; Dan, X.; Babbar, M.; Wei, Y.; Hasselbalch, S. G.; Croteau, D. L.; Bohr, V. A. Ageing as a risk factor for neurodegenerative disease. *Nat. Rev. Neurol.* **2019**, *15*, 565−581.

(2) Kalia, L. V.; Lang, A. E. Parkinson's disease. *Lancet* **2015**, *386*, 896−912.

(3) Kordower, J. H.; Olanow, C. W.; Dodiya, H. B.; Chu, Y.; Beach, T. G.; Adler, C. H.; Halliday, G. M.; Bartus, R. T. Disease duration and the integrity of the nigrostriatal system in Parkinson's disease. *Brain* **2013**, *136*, 2419−2431.

(4) Dong-Chen, X.; Yong, C.; Yang, X.; Chen-Yu, S.; Li-Hua, P. Signaling pathways in Parkinson's disease: molecular mechanisms and

therapeutic interventions. *Signal Transduction Targeted Ther.* **2023**, *8*, 73.
(5) Zhu, Y.; Ouyang, Z.; Du, H.; Wang, M.; Wang, J.; Sun, H.; Kong, L.; Xu, Q.; Ma, H.; Sun, Y. New opportunities and challenges of natural products research: When target identification meets single-cell multiomics. *Acta Pharm. Sin. B* **2022**, *12*, 4011−4039.
(6) Müller, T. Drug therapy in patients with Parkinson's disease. *Transl. Neurodegener.* **2012**, *1*, 10.
(7) Han, H.-H.; Tian, H.; Zang, Y.; Sedgwick, A. C.; Li, J.; Sessler, J. L.; He, X.-P.; James, T. D. Small-molecule fluorescence-based probes for interrogating major organ diseases. *Chem. Soc. Rev.* **2021**, *50*, 9391−9429.
(8) Quan, W.; Zhang, G.; Li, Y.; Song, W.; Zhan, J.; Lin, W. Upregulation of Formaldehyde in Parkinson's Disease Found by a Near-Infrared Lysosome-Targeted Fluorescent Probe. *Anal. Chem.* **2023**, *95*, 2925−2931.
(9) Wang, P.; Yu, L.; Gong, J.; Xiong, J.; Zi, S.; Xie, H.; Zhang, F.; Mao, Z.; Liu, Z.; Kim, J. S. An Activity-Based Fluorescent Probe for Imaging Fluctuations of Peroxynitrite ($ONOO^-$) in the Alzheimer's Disease Brain. *Angew. Chem., Int. Ed.* **2022**, *61*, No. e202206894.
(10) Gao, L.; Wang, W.; Wang, X.; Yang, F.; Xie, L.; Shen, J.; Brimble, M. A.; Xiao, Q.; Yao, S. Q. Fluorescent probes for bioimaging of potential biomarkers in Parkinson's disease. *Chem. Soc. Rev.* **2021**, *50*, 1219−1250.
(11) Zhang, K.; Sun, L.; Zhang, W.; Cao, M.; Ma, X.; Yu, B.-Y.; Xu, H.; Zheng, X.; Tian, J. Discovery of Natural Products Alleviating Renal Fibrosis with a Viscosity-Responsive Molecular Probe. *Anal. Chem.* **2024**, *96*, 6356−6365.
(12) Qin, Y.; Peng, C.; Yang, W.; Fan, J.; Sheng, W.-B.; Yi, P.; Qiu, Y.; Yu, H.; Jiang, S.; Wang, W.; Liu, B. A bi-functional fluorescent probe for visualized and rapid natural drug screening via GSTs activity monitoring. *Sensor Actuat B-Chem.* **2021**, *328*, 129047.
(13) Liu, K.; Zhang, J.; Li, X.; Xie, Y.; Li, Y.; Wang, X.; Jiao, X.; Xie, X.; Tang, B. Hypochlorous acid-activated two-photon fluorescent probe for evaluation of anticancer drug-induced cardiotoxicity and screening of antioxidant drugs. *Org. Chem. Front.* **2022**, *9*, 6795−6801.
(14) Yang, Y.-P.; Qi, F.-J.; Qian, Y.-P.; Bao, X.-Z.; Zhang, H.-C.; Ma, B.; Dai, F.; Zhang, S.-X.; Zhou, B. Developing Push−Pull Hydroxylphenylpolyenylpyridinium Chromophores as Ratiometric Two-Photon Fluorescent Probes for Cellular and Intravital Imaging of Mitochondrial NQO1. *Anal. Chem.* **2021**, *93*, 2385−2393.
(15) Mao, Z.; Xiong, J.; Wang, P.; An, J.; Zhang, F.; Liu, Z.; Seung Kim, J. Activity-based fluorescence probes for pathophysiological peroxynitrite fluxes. *Coord. Chem. Rev.* **2022**, *454*, 214356.
(16) Yang, Y.; Liu, X.; Xi, D.; Zhang, Y.; Gao, X.; Xu, K.; Liu, H.; Fang, M. Precision Imaging of Biothiols in Live Cells and Treatment Evaluation during the Development of Liver Injury via a Near-Infrared Fluorescent Probe. *Chem. Biomed. Imaging* **2024**, DOI: 10.1021/cbmi.4c00048.
(17) Feng, L.; Yang, Y.; Huo, X.; Tian, X.; Feng, Y.; Yuan, H.; Zhao, L.; Wang, C.; Chu, P.; Long, F.; Wang, W.; Ma, X. Highly Selective NIR Probe for Intestinal β-Glucuronidase and High-Throughput Screening Inhibitors to Therapy Intestinal Damage. *ACS Sens.* **2018**, *3*, 1727−1734.
(18) Chan, C.; Zhang, W.; Xue, Z.; Fang, Y.; Qiu, F.; Pan, J.; Tian, J. Near-Infrared Photoacoustic Probe for Reversible Imaging of the ClO^-/GSH Redox Cycle In Vivo. *Anal. Chem.* **2022**, *94* (15), 5918−5926.
(19) Zhang, K.; Sun, L.; Zhang, W.; Cao, M.; Ma, X.; Yu, B.-Y.; Xu, H.; Zheng, X.; Tian, J. Discovery of Natural Products Alleviating Renal Fibrosis with a Viscosity-Responsive Molecular Probe. *Anal. Chem.* **2024**, *96*, 6356.
(20) Deng, G.; Zhang, S.; Peng, X.; Ma, G.; Liu, L.; Tan, Y.; Gong, P.; Tang, B. Z.; Cai, L.; Zhang, P. Methylene Blue: An FDA-Approved NIR-II Fluorogenic Probe with Extremely Low pH Responsibility for Hyperchlorhydria Imaging. *Chem. Biomed. Imaging* **2024**, *2*, 683−688.
(21) Roberti, M. J.; Bertoncini, C. W.; Klement, R.; Jares-Erijman, E. A.; Jovin, T. M. Fluorescence imaging of amyloid formation in living cells by a functional, tetracysteine-tagged α-synuclein. *Nat. Methods* **2007**, *4*, 345−351.
(22) Li, H.; Xin, C.; Zhang, G.; Han, X.; Qin, W.; Zhang, C.-w.; Yu, C.; Jing, S.; Li, L.; Huang, W. A mitochondria-targeted two-photon fluorogenic probe for the dual-imaging of viscosity and H2O2 levels in Parkinson's disease models. *J. Mater. Chem. B* **2019**, *7*, 4243−4251.
(23) Fang, H.; Zhang, H.; Li, L.; Ni, Y.; Shi, R.; Li, Z.; Yang, X.; Ma, B.; Zhang, C.; Wu, Q.; Yu, C.; Yang, N.; Yao, S. Q.; Huang, W. Rational Design of a Two-Photon Fluorogenic Probe for Visualizing Monoamine Oxidase A Activity in Human Glioma Tissues. *Angew. Chem., Int. Ed.* **2020**, *59*, 7536−7541.
(24) Bae, S. K.; Heo, C. H.; Choi, D. J.; Sen, D.; Joe, E.-H.; Cho, B. R.; Kim, H. M. A Ratiometric Two-Photon Fluorescent Probe Reveals Reduction in Mitochondrial H2S Production in Parkinson's Disease Gene Knockout Astrocytes. *J. Am. Chem. Soc.* **2013**, *135*, 9915−9923.
(25) Gong, J.; Wang, X.; Wu, J.; Yoon, C.; Kim, Y.; Zou, J.; Mao, Z.; Kim, J. S. Diaminonaphthalene Boronic Acid (DANBA): New Approach for Peroxynitrite Sensing Site. *Angew. Chem., Int. Ed.* **2024**, *63*, No. e202409295.
(26) Wang, X.; He, S.; Cheng, P.; Pu, K. A Dual-Locked Tandem Fluorescent Probe for Imaging of Pyroptosis in Cancer Chemo-Immunotherapy. *Adv. Mater.* **2023**, *35*, 2206510.
(27) Hu, J.-s.; Shao, C.; Wang, X.; Di, X.; Xue, X.; Su, Z.; Zhao, J.; Zhu, H.-L.; Liu, H.-K.; Qian, Y. Imaging Dynamic Peroxynitrite Fluxes in Epileptic Brains with a Near-Infrared Fluorescent Probe. *Adv. Sci.* **2019**, *6*, 1900341.
(28) Zhang, W.; Chan, C.; Zhang, K.; Qin, H.; Yu, B.-Y.; Xue, Z.; Zheng, X.; Tian, J. Discovering a New Drug Against Acute Kidney Injury by Using a Tailored Photoacoustic Imaging Probe. *Adv. Mater.* **2024**, *36*, 2311397.
(29) Qian, M.; Wang, K.; Yang, P.; Liu, Y.; Li, M.; Zhang, C.; Qi, H. Nonemissive Iridium(III) Solvent Complex as a Self-Reporting Photosensitizer for Monitoring Phototherapeutic Efficacy in a "Signal on" Mode. *Chem. Biomed. Imaging* **2024**, DOI: 10.1021/cbmi.4c00042.
(30) Xiong, J.; Wang, W.; Wang, C.; Zhong, C.; Ruan, R.; Mao, Z.; Liu, Z. Visualizing Peroxynitrite in Microvessels of the Brain with Stroke Using an Engineered Highly Specific Fluorescent Probe. *ACS Sens.* **2020**, *5*, 3237−3245.
(31) Li, Y.; Cao, J.; Wu, X.; Kou, J.; Feng, T.; Zhang, R.; Xu, C.; Kong, F.; Tang, B. A Sequentially Activated Probe for Imaging of Superoxide Anion and Peroxynitrite in PC12 Cells under Oxidative Stress. *Anal. Chem.* **2024**, *96*, 7138−7144.
(32) Cheng, J.; Li, D.; Sun, M.; Wang, Y.; Xu, Q.-Q.; Liang, X.-G.; Lu, Y.-B.; Hu, Y.; Han, F.; Li, X. Physicochemical-property guided design of a highly sensitive probe to image nitrosative stress in the pathology of stroke. *Chem. Sci.* **2020**, *11*, 281−289.
(33) Sun, Q.; Xu, J.; Ji, C.; Shaibani, M. S. S.; Li, Z.; Lim, K.; Zhang, C.; Li, L.; Liu, Z. Ultrafast Detection of Peroxynitrite in Parkinson's Disease Models Using a Near-Infrared Fluorescent Probe. *Anal. Chem.* **2020**, *92*, 4038−4045.
(34) Yan, M.; Fang, H.; Wang, X.; Xu, J.; Zhang, C.; Xu, L.; Li, L. A two-photon fluorescent probe for visualizing endoplasmic reticulum peroxynitrite in Parkinson's disease models. *Sensor Actuat B-Chem.* **2021**, *328*, 129003.
(35) Kang, H.; Shu, W.; Yu, J.; Gao, M.; Han, R.; Jing, J.; Zhang, R.; Zhang, X. A near-infrared fluorescent probe for ratiometric imaging peroxynitrite in Parkinson's disease model. *Sensor Actuat B-Chem.* **2022**, *359*, 131393.
(36) Sun, X.; Jiang, Q.; Zhang, Y.; Su, J.; Liu, W.; Lv, J.; Yang, F.; Shu, W. Advances in fluorescent probe development for bioimaging of potential Parkinson's biomarkers. *Eur. J. Med. Chem.* **2024**, *267*, 116195.
(37) Gao, L.; Wang, W.; Wang, X.; Yang, F.; Xie, L.; Shen, J.; Brimble, M. A.; Xiao, Q.; Yao, S. Q. Fluorescent probes for bioimaging of potential biomarkers in Parkinson's disease. *Chem. Soc. Rev.* **2021**, *50*, 1219−1250.
(38) Kang, H.; Shu, W.; Yu, J.; Gao, M.; Han, R.; Jing, J.; Zhang, R.; Zhang, X. A near-infrared fluorescent probe for ratiometric imaging

peroxynitrite in Parkinson's disease model. *Sensor Actuat B-Chem.* **2022**, *359*, 131393.
(39) Yan, M.; Fang, H.; Wang, X.; Xu, J.; Zhang, C.; Xu, L.; Li, L. A two-photon fluorescent probe for visualizing endoplasmic reticulum peroxynitrite in Parkinson's disease models. *Sensor Actuat B-Chem.* **2021**, *328*, 129003.
(40) Li, S.; Wang, P.; Feng, W.; Xiang, Y.; Dou, K.; Liu, Z. Simultaneous imaging of mitochondrial viscosity and hydrogen peroxide in Alzheimer's disease by a single near-infrared fluorescent probe with a large Stokes shift. *Chem. Commun.* **2020**, *56*, 1050−1053.
(41) Miao, J.; Miao, M.; Jiang, Y.; Zhao, M.; Li, Q.; Zhang, Y.; An, Y.; Pu, K.; Miao, Q. An Activatable NIR-II Fluorescent Reporter for In Vivo Imaging of Amyloid-β Plaques. *Angew. Chem., Int. Ed.* **2023**, *62*, No. e202216351.
(42) Jiang, Z.; Liang, Z.; Cui, Y.; Zhang, C.; Wang, J.; Wang, H.; Wang, T.; Chen, Y.; He, W.; Liu, Z.; Guo, Z. Blood−Brain Barrier Permeable Photoacoustic Probe for High-Resolution Imaging of Nitric Oxide in the Living Mouse Brain. *J. Am. Chem. Soc.* **2023**, *145*, 7952−7961.
(43) Mao, Z.; Kim, J. H.; Lee, J.; Xiong, H.; Zhang, F.; Kim, J. S. Engineering of BODIPY-based theranostics for cancer therapy. *Coord. Chem. Rev.* **2023**, *476*, 214908.
(44) Wang, C.; Sun, Y.; Huang, S.; Wei, Z.; Tan, J.; Wu, C.; Chen, Q.; Zhang, X. Self-Immolative Photosensitizers for Self-Reported Cancer Phototheranostics. *J. Am. Chem. Soc.* **2023**, *145*, 13099−13113.
(45) Wang, S.; Gai, L.; Chen, Y.; Ji, X.; Lu, H.; Guo, Z. Mitochondria-targeted BODIPY dyes for small molecule recognition, bio-imaging and photodynamic therapy. *Chem. Soc. Rev.* **2024**, *53*, 3976−4019.
(46) Chen, N.; Zhang, W.; Chen, S.; Wu, Q.; Yu, C.; Wei, Y.; Xu, Y.; Hao, E.; Jiao, L. Sterically Protected N2O-Type Benzopyrromethene Boron Complexes from Boronic Acids with Intense Red/Near-Infrared Fluorescence. *Org. Lett.* **2017**, *19*, 2026−2029.
(47) Wang, W.; Xiong, J.; Song, X.; Wang, Z.; Zhang, F.; Mao, Z. Activatable Two-Photon Near-Infrared Fluorescent Probe Tailored toward Peroxynitrite In Vivo Imaging in Tumors. *Anal. Chem.* **2020**, *92*, 13305−13312.
(48) Gong, J.; Wang, X.; Fan, H.-E.; Wang, J.; Zhang, F.; Mao, Z. Engineering an activatable fluorescent probe for studying $ONOO^-$ in pyroptotic process. *Talanta* **2024**, *267*, 125216.
(49) Kim, Y. L.; Plank, J. T.; Li, B.; Lippert, A. R. Kinetics-Based Quantification of Peroxynitrite Using the Oxidative Decarbonylation of Isatin. *Anal. Chem.* **2022**, *94*, 17803−17809.
(50) Yang, Y.; Zhang, Y.; Ma, M.; Liu, H.; Ge, K.; Zhang, C.; Jin, M.; Liu, D.; Wang, S.; Yin, C.; Zhang, J. Synergistic Modulation by Halogens and Pyridine Crossing the Blood−Brain Barrier for In Situ Visualization of Thiol Flux in the Epileptic Brain. *Anal. Chem.* **2022**, *94*, 14443−14452.
(51) Wu, L.; Liu, J.; Tian, X.; Groleau, R. R.; Feng, B.; Yang, Y.; Sedgwick, A. C.; Han, H.-H.; Wang, Y.; Wang, H.-M.; Huang, F.; Bull, S. D.; Zhang, H.; Huang, C.; Zang, Y.; Li, J.; He, X.-P.; Li, P.; Tang, B.; James, T. D.; Sessler, J. L. Dual-Channel Fluorescent Probe for the Simultaneous Monitoring of Peroxynitrite and Adenosine-5′-triphosphate in Cellular Applications. *J. Am. Chem. Soc.* **2022**, *144*, 174−183.
(52) Ferrer-Sueta, G.; Campolo, N.; Trujillo, M.; Bartesaghi, S.; Carballal, S.; Romero, N.; Alvarez, B.; Radi, R. Biochemistry of Peroxynitrite and Protein Tyrosine Nitration. *Chem. Rev.* **2018**, *118*, 1338−1408.
(53) Peng, T.; Chen, X.; Gao, L.; Zhang, T.; Wang, W.; Shen, J.; Yang, D. A rationally designed rhodamine-based fluorescent probe for molecular imaging of peroxynitrite in live cells and tissues. *Chem. Sci.* **2016**, *7*, 5407−5413.
(54) Deng, Y.; Shi, X.; Hu, X.; Xu, L.; Liu, X.; Gao, G.; Wang, R.; Liang, G. A Chemiluminescent Probe for Imaging Peroxynitrite in Inflammatory Cells and Tissues. *Anal. Chem.* **2023**, *95*, 6496−6500.
(55) Schildknecht, S.; Di Monte, D. A.; Pape, R.; Tieu, K.; Leist, M. Tipping Points and Endogenous Determinants of Nigrostriatal Degeneration by MPTP. *Trends Pharmacol. Sci.* **2017**, *38*, 541−555.
(56) Kartik, S.; Pal, R.; Chaudhary, M. J.; Nath, R.; Kumar, M.; Binwal, M.; Bawankule, D. U. Neuroprotective role of chloroquine via modulation of autophagy and neuroinflammation in MPTP-induced Parkinson's disease. *Inflammopharmacology* **2023**, *31*, 927−941.
(57) Muhammad, F.; Liu, Y.; Zhou, Y.; Yang, H.; Li, H. Antioxidative role of Traditional Chinese Medicine in Parkinson's disease. *J. Ethnopharmacol.* **2022**, *285*, 114821.
(58) Chen, J.; Xu, J.; Huang, P.; Luo, Y.; Shi, Y.; Ma, P. The potential applications of traditional Chinese medicine in Parkinson's disease: A new opportunity. *Biomed. Pharmacother.* **2022**, *149*, 112866.

https://doi.org/10.1021/cbmi.4c00076
Chem. Biomed. Imaging 2025, 3, 301−309